IEEE Open Journal of
Power Electronics

Received 27 February 2026; revised 17 April 2026; accepted 22 April 2026. Date of publication 30 April 2026;
date of current version 20 May 2026. The review of this article was arranged by Associate Editor Hongbo Zhao.

Digital Object Identifier 10.1109/OJPEL.2026.3689194

Optimal Technical-Economic Design of a DC Microgrid for Electroplating Industry

STEFANO LILLA [1] (Member, IEEE), ANDREA ALESSIA TAVAGNUTTI [2] (Member, IEEE), DANIELE BOSICH [2] (Senior Member, IEEE), FABIO NAPOLITANO [1] (Senior Member, IEEE), ANDREA PREVEDI [1], FABIO TOSSANI [1] (Senior Member, IEEE), GIORGIO SULLIGOI [2] (Senior Member, IEEE), AND CARLO ALBERTO NUCCI [1] (Life Fellow, IEEE)

[1]Department of Electrical, Electronic, and Information Engineering "Guglielmo Marconi", University of Bologna, 40136 Bologna, Italy
[2]Department of Engineering and Architecture, University of Trieste, 34127 Trieste, Italy

CORRESPONDING AUTHOR: DANIELE BOSICH (e-mail: dbosich@units.it)

This work was supported by the Italian Ministry for University and Research through "Network 4 Energy Sustainable Transition - NEST" Project MUR Project PE000021, Concession Decree No. 1561 of 11.10.2022, within the framework of the NextGenerationEu PNRR plan under Grant CUP J33C22002890007. An earlier version of this paper was presented at the 2025 IEEE 7th International Conference on DC Microgrids (ICDCM), Tallin, Estonia [DOI: 10.1109/ICDCM63994.2025.11144681].

ABSTRACT The paper proposes the implementation of a controlled DC microgrid to supply DC loads in a plating industry. The plating loads, typically from chromium-based surface coating processes, are characterized by low voltage (10–20 V) and high currents (5–10 kA). To adopt renewable sources, the supplying 600 V-DC microgrid is powered by a photovoltaic (PV) system and a Battery Energy Storage (BES) system. Main aim of the work is to develop a smart strategy to reduce energy consumption, while lowering electricity costs, and minimizing the current ripple affecting the loads. Since PV systems cannot provide a continuous power supply, the system also includes an interface with the external AC grid by a bidirectional DC/AC converter. This hybrid converter allows to feed back the PV energy excess to the grid, still ensuring electricity supply when needed. The paper wants to provide a technical-economic overview, from the sizing of PV and BES systems to the voltage control system, including an Energy Management System (EMS). In particular, the study is aimed at determining the optimal PV system size and BES capacity size to maximize the Net Present Value (NPV) of investments-originated savings. Industrial electricity load profiles, PV generation data derived from 18 years of average hourly irradiation, and three years of electricity price profiles are adopted as optimization inputs. Particularly, the BES power is optimized over a one-year period to minimize grid energy exchange, with annual cost curves to maximize the NPV. Finally, with the same MILP approach as sizing, an EMS with real-time control is proposed in the optimization of microgrid devices, while the DC voltage control system is discussed in detail with tests performed on a Hardware In the Loop (HIL) platform in some scenarios among equilibrium conditions. The paper aims to make a contribution to the development of energy management strategies for reducing procurement costs in industries that make extensive use of DC current, suggesting the entire process, from the optimal calculation of the sizing of the components, to the daily management of the microgrid with optimized scheduling of the EMS, including the control system.

INDEX TERMS DC microgrid, electroplating, EMS, galvanic industry, national price, net present value NPV optimization, optimal size, voltage control system.

NOMENCLATURE

T	set of optimization periods t, each of duration Δt.
π_{exp}, π_{in}	selling and purchasing energy prices.
P_{grid_ex}, P_{grid_in}	exchange meter power injection - absorption.
P_{PV}	power injection by PV production.
P_{load}	power absorbed by the loads.

PV^{size}	size of the photovoltaic facility.
E_t^S	shared energy.
P_{BES_di}, P_{BES_ch}	discharge and charge BES power.
P_{BES}	BES power, limited between $P_{\mathrm{BES,min}}$, $P_{\mathrm{BES,max}}$.
$E_{BES,\max}$	BES capacity.
SOC	BES State Of Charge.
$\eta_{AC/DC}$	bidirectional grid interface converter efficiency.
η_{BES}	storage charging and discharging efficiency.
C	annual cost of electricity.
$C_{(0)}$	annual cost of electricity without PV and BES system.
C_{PV}	total annual cost of electricity with PV, without BES.
$C_{(BES)}$	total annual cost of electricity with PV and BES.
$C_{O\&M}$	annual cost for operations/maintenance of PV and BES systems (OPEX).
C_{PV_SIZE}	total annual cost of electricity as a function of the PV size.
S_{PV_SIZE}	total annual savings with PV as a function of PV size.
C_{BES_SIZE}	total annual cost of electricity as a function of BES size.
S_{BES_SIZE}	total annual savings with BES as a function of the BES size.
D	degradation rate of the capacity BES.
T_{PV}, T_{BES}	is the useful life of the PV/BES system in years.
C_{O_PV}, C_{O_BES}	initial cost to install PV/BES system (CAPEX).
r	discount rate.

I. INTRODUCTION

Last years, the European Union has implemented a comprehensive policy framework to facilitate the energy transition and the affordable use of electricity. This legislation includes both ambitious renewable energy targets outlined in the Renewable Energy Directive II (RED II) [1], and stringent regulations governing energy efficiency and consumption across all sectors, as well as industrial processes [2]. Under the "Fit for 55" package, the Energy Efficiency Directive (EED) [3] establishes binding targets that directly shape industrial energy strategies. Indeed, it obliges large enterprises either to implement energy management or to conduct regular energy audits.

Thanks to the increasing exploitation of renewable energy sources interfaced with power converters, in urban, residential, and industrial plans, the possibility of using DC microgrids is being taken into consideration more often. In this context, the DC MGs provide several advantages compared to AC MGs. To give a short list, it is possible to enumerate improved efficiency, better control, stability, compatibility with the DC nature of renewables and storage sources, and the absence of reactive power and synchronization [4]. On the other hand, a review on the issues of DC MGs (e.g., architecture, protection, power quality, inertia, communication, and economic operation) is in [5] to give a complete background on this technology.

TABLE 1. Main Processes Suitable for DC Microgrids [8]

Industry	Power Range (kW)	Typical DC Voltage Level
Electrolysis & Metal Processing Small-scale facilities	10 - 1000	2–50 V (low voltage for electrochemical reactions)
Arc Welding Shielded Metal Arc Weld TIG Welding Plasma Cutting	1 – 200 2 – 50 5 – 200	20–100 V (depends on welding method and materials)
Semiconductor Fabs Thin-Film Deposition	10 – 100	48 V – 600 V (varies across processes)
Data Centers Small-scale facilities	100 – 1000	12-48 V servers, 400 V systems
Electrolysis Small-scale facilities	100 – 1000	1.8 – 2.2 volts per cell Hundreds V for systems

In general, certain industrial processes are particularly well-suited for controlled DC distribution, forming the basis of DC MGs [6], [7]. A summary of the most interesting applications [8] as DC microgrids is in Table 1, where usual power-voltage values are reported.

Electroplating is one process where DC microgrids are suggested. This technique is employed to deposit a thin, uniform layer of metal onto the surface of metal objects [9]. This galvanic process is commonly used to enhance corrosion resistance, while improving the aesthetic appeal of artifacts. This paper investigates on an industrial facility specialized in chromium-based coatings for steel pipes. The coating process involves electrolytic deposition, where a DC-polarized electrolysis cell is adopted [9].

To activate the reactions and thus energize the electroplating tank, generally, an AC/DC rectifier converter is interfaced to the main supply (400 V/50 Hz). Four primary power supply types with rectifiers were historically used: 1) variable transformers with rectifier, 2) silicon-controlled rectifier (SCR), 3) step-down transformer with linear rectifier, and 4) switching power supply [10]. This type of converter is characterized by the presence of harmonics on the grid side, large energy loss, low power factor and high ripple current [11]. In electroplating applications, minimizing ripple current is of primary importance. A stable electroplating bath (i.e., consistent temperature and pH) is indeed essential for achieving high-quality coatings. By preventing fluctuations in the electrical current supplied to the bath, the ripple current reduction can contribute in guaranteeing a stable bath. It is thus necessary to keep the current density injected into the tank as constant as possible. To achieve high-quality chrome plating, it is important to apply high current and voltage with minimal ripple. Consequently, rectifiers in chrome plating must exhibit lower ripple-higher capacity compared to those in other metal plating processes [9], [11], [12]. To complete the context, in

a production facility multiple DC powered electrodeposition tanks are installed. The latter are typically supplied with voltage between 10 V and 20 V and very high currents (from 5 kA to 10 kA). During the day, the power grid could be powered using a PV system on the building roof. The employment of controlled DC MG constitutes the smartest and most efficient approach to manage a system powered by renewable and storage [13]. For these types of plants, identifying the optimal integration of PV system and BES is crucial for maximizing the Net Present Value (NPV) of investment-originated savings to have the optimal size.

Although several works have dealt with the sizing of combined PV and Battery Energy Storage (BES) solutions. In [14] the scheduling and the economic analysis was performed to determine the size of the BES maximizing mainly the Renewable Energy Certificate profit and the System Marginal Price profit. The paper [15] presents an LP optimization (excluding integer variables) for the dispatch scheduling and economic assessment of PV systems coupled with BES; economic performance is assessed through simple payback time and net savings, rather than NPV maximization. In [16] the authors propose a multi-objective optimization framework that explicitly balances economic performance and investment scale for BES sizing; the non-convex model generate a Pareto front, allowing decision-makers to identify trade-offs between profitability and capital intensity.

When adopting a DC microgrid, the efficient operation relies on the deployment of an Energy Management System (EMS) [17], [18]. The latter enables the effective integration of DC-native renewable energy sources and BES systems with minimal conversion stages and reduced associated losses. To achieve predefined operational goals, EMSs typically account for factors such as energy price forecasts, renewable generation availability, and load prioritization [19]. In the literature, numerous objective functions (OFs) have been proposed, with one of the most common focusing on the minimization of energy procurement costs [20]. To address these optimization problems, different techniques have been employed (e.g., [21]), among which Mixed-Integer Linear Programming (MILP) has emerged as a particularly effective and versatile approach [17].

In the proposed planning framework, PV capacity is optimized prior to BES sizing rather than through a fully joint PV–BES co-optimization. Assuming that the system is grid-connected and without curtailment, that the marginal cost of PV is about zero, that monotonic relationship between PV and BES capacity (as will be seen later – Fig. 10 – the trend is linear), that the system is not able to influence the NPV market price and that BES revenue depends mainly by price volatility, the sequential PV–BES sizing remains near-optimal. In industrial applications dominated by self-consumption, PV sizing is primarily driven by load profiles and available installation constraints, while the marginal economic value of the BES depends mainly on price volatility and residual surplus energy. The coupling between optimal PV size and BES value with joint optimization would substantially increase computational complexity without yielding materially different sizing outcomes for the scenarios considered.

A. CONTRIBUTION OF THE PAPER AND METHODOLOGY

This paper investigates the introduction of a DC microgrid (MG) in industrial environments that already make extensive use of direct current, such as electroplating plants, an application area that, to the authors' knowledge, has not been previously addressed in literature. The analysis adopts a comprehensive perspective: first, the optimal sizing of generation unit and the BES is assessed; subsequently, microgrid operation and energy management system (EMS) control strategies are evaluated, providing insights relevant to real-time implementation.

Compared to existing studies, a two-step MILP-based optimization framework is employed for capacity sizing, offering robustness and transparency for investment-oriented decision-making. In the first step, annual BES scheduling is optimized using 18 years of historical PV production data and considering the National Single Price (NSP) of three representative years: 2021 (low prices), 2022 (high prices), and 2023 (low prices). The MILP-based program is developed with the specific objective of minimizing energy procurement costs. The resulting operating costs are then used in the second step to derive and linearize the cost curve, ensuring a convex optimization problem suitable for economic sizing. This linearized cost-based sizing approach is not commonly adopted in existing literature. The linearized curve is the input for the second optimization step which aims to maximize NPV and choose the corresponding optimal size. Then, a sensitivity analysis evaluates the impact of load variability (modeled through multiples of the load standard deviation), discount rate, and BES degradation over time (assumed linear) on the optimal storage size. A specific study on the DC voltage control testifies how the controlled microgrid can proficiently work both in islanded and interconnected mode. Particular attention is spent on the transition between one operative mode and the other, when indeed PV and batteries operate properly for the green supply of the electroplating process. To integrate day-ahead optimization into the EMS, the same MILP formulation used in Step 1 is adopted, with the time horizon reduced to 24 hours (96 periods), with the same objective of minimizing the energy procurement cost. In addition, the EMS employs a hierarchical architecture with day-ahead scheduling and a real-time receding-horizon control layer to correct forecast deviations in PV generation and load. Corrective actions adjust BES and grid power setpoints while preserving long-term economic decisions and system constraints.

The main contributions of this paper can be summarized as follows:

- The study addresses the integration of a DC microgrid in electroplating processes, an industrial application that has not been explicitly investigated in existing PV–BES literature.
- Sizing methodology: A two-step MILP-based optimization framework is proposed, in which long-term

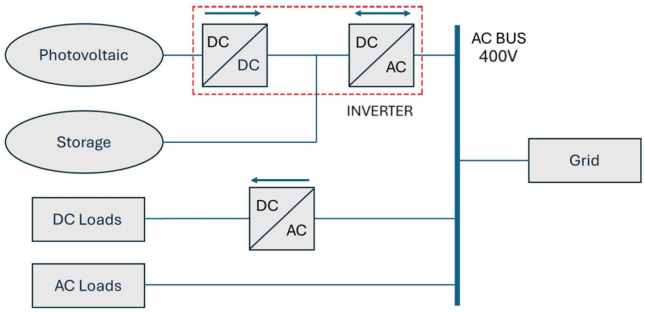

FIGURE 1. One line diagram of a standard AC distribution system containing PV and BES.

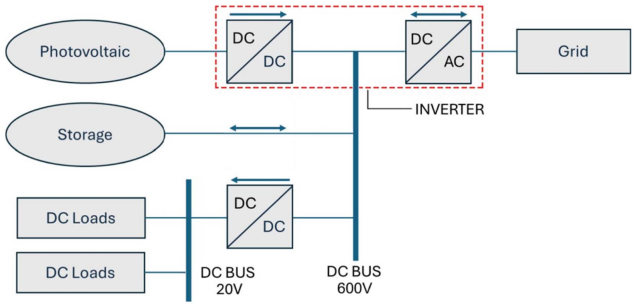

FIGURE 2. One line diagram of the proposed DC distribution system.

operational scheduling is first used to derive cost functions, subsequently embedded in an NPV-based sizing problem through a linearized formulation.

- Decoupled optimization approach: The separation between operational scheduling and investment decisions enables improved computational efficiency and transparency, while maintaining near-optimal sizing results.
- The framework incorporates long-term PV production data (18 years) and representative market price scenarios to capture realistic variability.
- The proposed sizing methodology is coherently linked to a hierarchical EMS architecture, including day-ahead optimization and a receding-horizon (MPC-like) control strategy for real-time operation.
- The impact of key parameters, including discount rate, BES degradation, and load variability, is systematically evaluated.
- The control architecture is compatible with hardware-in-the-loop (HIL/CHIL) environments, supporting practical validation.

The paper structure is in the following. Section II is devoted to the description of DC MG configurations for considered industrial process. Section III presents the problem formulation and the description of the MILP model to optimize the NPV. Section IV illustrates the results of numerical tests obtained by NPV optimization. In Section V, DC voltage control and Typhoon HIL results are discussed. Section VI describes the MILP model to be included in the EMS and real-time control. Section VII concludes the paper.

II. DC MICROGRID CONFIGURATION FOR ELECTROPLATING

As reported in [22] in an electroplating industry the installed load (i.e., electrodeposition tanks) requires DC low-voltage high-current. As in Fig. 1, a first idea envisages that such a load is supplied by both the AC network and also by a PV system. In this standard distribution, the PV system is thus connected to the 400 V AC bus through a solar inverter, and in turn, the AC bus supplies the electroplating tanks through an AC/DC rectifier. Because of the high current and significant cost, such rectifiers lack output filtering and therefore produce a noticeable current ripple [23].

Conversely, in the present work a 600 V DC bus interconnecting the DC side of converters is proposed constituting an innovative microgrid system configuration for this kind of industry. This MG is supplied by the DC output of the hybrid inverter, normally used to connect to the BES only. Therefore, it is used to power the DC load, as well as to interface the BES and internal DC/DC converter (Fig. 2). In other words, this is a matter of extending the DC output section of the inverter to the load, wired in parallel with the BES. Two pieces of equipment (i.e., rectifier and inverter) are thus replaced by a single one, the solar hybrid inverter. In close proximity to the loads (of working voltage 10 V to 20 V and current 10 kA), DC/DC converters will be installed to step-down the voltage to the required level (Fig. 2). This high-efficiency converter also provides galvanic isolation between the two voltage levels [24]. The proposed diagram features two DC buses. Firstly, a high voltage bus (600 V), designed to integrate power generated by the PV strings into the system and facilitate energy exchange with the BES. Secondly, a low voltage bus (20 V), dedicated to supply power to the electrochemical tanks, while minimizing energy distribution within the factory. For the main DC bus to interface the BES, the voltage level is assumed to be 600 V, therefore a typical value of commercially available inverters. Furthermore, such a value is compatible with the AC grid voltage, which has a peak value of 556 Vp (400 Vrms).

In electroplating industry, the ripple reduction constitutes an important target to be attained. A low frequency ripple can indeed deteriorate the desired output in electroplating process [25]. In addition to these considerations, the work in [26], also demonstrates how the filtering arrangement for a high frequency application (i.e., DC/DC converter) is smaller in size (−75%) compared to the solutions in low frequency (i.e., thyristor AC/DC rectifier). This aspect is remarkable in electroplating [27]. The AC solution (Fig. 1) employs a conventional three-phase six-pulse bridge rectifier to supply the electroplating load, whereas the DC solution (Fig. 2) utilizes a DC-DC converter. The primary advantage of the DC-DC stage lies in the frequency shift of the ripple components. Specifically, a passive rectifier exhibits a dominant ripple frequency of 6fs [28], which corresponds to 300 Hz (assuming a 50 Hz supply). In contrast, DC-DC converters operate at switching frequencies ranging from the kHz scale

to tens of MHz. While the theoretical voltage ripple factor for a six-pulse rectifier is approximately 4.2% [29], the current ripple in electroplating loads often exceeds 10% without filtering. This level is unacceptable for high-precision electroplating processes, necessitating bulky filtering components. Conversely, in DC-DC converters, voltage and current ripples can be minimized not only through appropriate filter design but also by adopting specific topologies and control strategies (e.g., interleaving) to enhance power quality [30]. Specifically, the current ripple magnitude is inversely proportional to the switching frequency (i.e., $\Delta I = \frac{(V_{in}-V_{out})\cdot D}{L\cdot f_s}$) and can be further reduced below 5% using advanced techniques [31]. Since the quality of the electrochemical deposition depends directly on the output current, the ripple on the DC side is the critical performance metric for this application. The proposed configuration brings some other advantages as expressed in the following: during daylight, the PV system (by means of the DC/DC section of the hybrid inverter) can directly supply the DC bus avoiding a double conversion; at night or during unfavorable weather, the same hybrid inverter (AC/DC section) can supply the load by drawing power from the AC network; therefore, a double conversion is avoided if the BES inject power. As the high ripple is mainly given by unfiltered AC/DC rectification [23], a significant reduction in ripple is reached by excluding the load rectifier from the system. This proposed configuration also beneficially utilizes widely available technologies, i.e., hybrid inverters. Secondary loads (mainly lighting) will be therefore powered in DC to avoid distributing the AC bus. In general, the introduction of a 600 V_{DC} microgrid in an industrial facility originally designed for a 400 V_{AC} supply requires careful consideration of standards, safety, and load compatibility (e.g., IEC 60364 - *Low-voltage electrical installations*). In particular, conventional AC lighting systems cannot be directly supplied by DC and must be replaced with DC-compatible luminaires (e.g., IEC 60598 - *Luminaires*, IEC 62031 - *LED modules for general lighting*). DC systems also require specific protection devices, grounding schemes, and arc-fault mitigation strategies, as fault behavior differs significantly from AC systems (e.g., IEC 60269 - *Low-voltage fuses*).

The inverters firmware usually controls the PV production by adopting Maximum Power Point Tracking (MPPT) strategy, thus it ensures the interface with the external AC grid and regulates BES charge/discharge as a function of the AC load. In this case, the algorithm also is to be interfaced with both global EMS and DC loads, with related data for optimally charging/discharging the BES. Although commercial hybrid inverters and high-power isolated DC/DC converters are available, their deployment in electroplating plants poses practical challenges due to the combination of kiloampere-level currents and very low DC voltages (10–20 V). Individual converter ratings are typically insufficient for direct kA operation, requiring extensive parallelization, which complicates current sharing, thermal management, and busbar design while amplifying the impact of conduction losses and voltage drops. In addition, DC fault protection and selectivity at high currents remain challenging and require careful coordination between upstream hybrid converters and downstream DC/DC stages. Compared to conventional rectifier-based solutions, the proposed architecture also increases system coordination and maintenance complexity, necessitating conservative derating, robust control strategies, and alignment with industrial reliability and availability requirements.

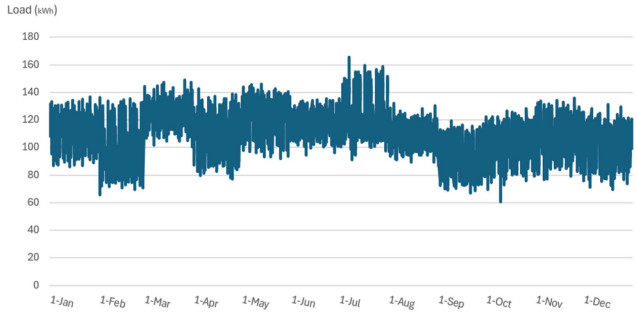

FIGURE 3. Hourly profile of the electrical load in 2023.

III. NPV OPTIMIZATION APPROACH

The DC MG is a radial system where PV plant, BES, main grid and loads are interconnected. The optimization algorithm aims to first determine the optimal size of PV system that maximizes the NPV accounting for plant construction CAPEX. Subsequently, it defines the optimal size of the BES to maximize the NPV, factoring in the CAPEX for its acquisition.

A. INPUT DATA

The annual MILP is deterministic and does not explicitly model stochastic forecasting errors. Long-term uncertainty is addressed through multi-year PV production data and representative market scenarios, enabling robust sizing decisions that capture interannual variability while providing a stable basis for investment-oriented optimization. Then, uncertainty is represented indirectly by using long-term average PV data and by injecting Gaussian perturbations into the load profile, complemented by a sensitivity analysis. the following data will be used to optimize the system.

- The hourly profile of electrical power consumed in 2023 is in Fig. 3. Lacking real measured hourly power consumption data for the specific electroplating factory, data relating to monthly energy consumption were used. However, in order to simulate a more realistic scenario that includes hourly load fluctuations, the variability of power absorption has been modelled by applying a random change to the average active power data, such that peak power and total energy absorbed are unvaried.
- The profile of the electrical power produced by each kWp of PV system on the rooftop, inferred by the total hourly irradiation using PVGIS (from JRC). This evaluation is made by considering the average of the last 18 years) related to the site of interest (province of Bologna, Italy).

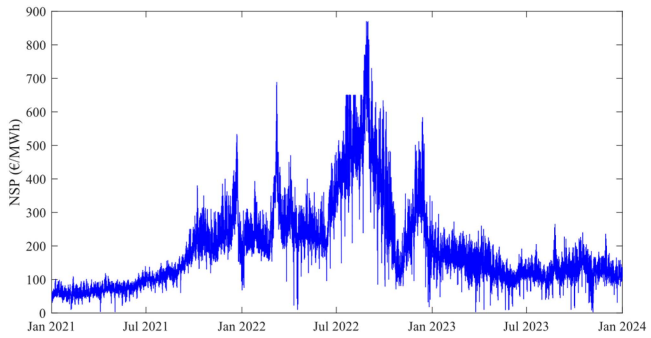

FIGURE 4. NSP hourly profile in 2021, 2022 and 2023.

- The hourly profile of the National Single Price (NSP) considering the years 2021, 2022 and 2023. These years are selected to catch two distinct market price regimes relevant to the analysis: 2021 and 2023 represents a low-price regime, and 2022 a high-price regime, thereby enabling a comparative assessment of BES performance across differing market conditions, as highlighted in Fig. 4 [32].

The total cost of electricity (sum of the amount of bills) in the last year taking into account the process. In electroplating, the pieces to be chromed are immersed in large tanks (electric loads), the processing takes place in a continuous cycle and in turn the tanks are loaded and unloaded one at a time. So only part of the load is variable during the 24 hours. To account for this variability in load demand, the profile is constructed by applying a Gaussian noise. In the sensitivity analysis, to better evaluate the load variability, the effect on the system is considered by varying the standard deviation between 1 and 5. In addition, additional assumptions are to be put: the energy injected into the grid is valued at the hourly NSP (the energy component, on average, makes up 50% of the cost of the bill); the discount rate is set at 3% and adequate efficiency for converters and BES is considered. In PV system, a loss of efficiency equal to −1%/year is considered.

B. OPERATION CONSTRAINTS

Some constraints are assumed as in the following. The DC-bus power balance is in (1), while the net power exchanged with the main grid is given by (2) in the cases of imported/exported power:

$$P_{load} + P_{BES} = P_{grid} + P_{PV} \tag{1}$$

$$\begin{cases} P_{grid\_in} = \eta_{AC/DC} P_{grid} \\ -P_{grid\_ex} = P_{grid} / \eta_{AC/DC} \end{cases} \tag{2}$$

The BES power P_{BES} is assumed to be positive during the charging phase. To avoid simultaneous injection and absorption of power from the grid in the same period, a binary variable v is introduced:

$$\begin{cases} P_{grid\_in} \leq v \cdot P_{grid\_in\_MAX} \\ P_{grid\_ex} \leq (1 - v) \cdot P_{grid\_ex\_MAX} \end{cases} \tag{3}$$

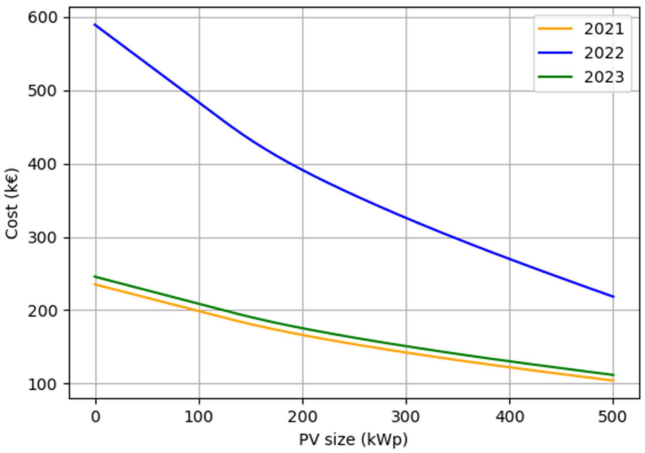

FIGURE 5. Energy cost as a function of the PV size (from 0 to 500 kWp) considering NSP of 2021, 2022 and 2023 [22].

C. OPTIMAL PV SIZE

Before calculating the NPV, the energy procurement cost curve is modeled as a function of PV size, incorporating the annual marginal savings achieved by progressively increasing the PV capacity. The cost curve is defined as $S^{PV\_SIZE} = C_{(0)} - C_{PV\_SIZE}$. For each PV size (from 0 to 500 kWp), the calculation in (4) is thus done:

$$C = \sum_{t=0}^{T} (P_{grid\_in,\,t} \cdot \pi_{in,\,t} - P_{grid\_ex,\,t} \cdot \pi_{ex,\,t}) \cdot \Delta t \tag{4}$$

The resulting cost curve in Fig. 5 is non-linear, making the optimization system non-linear too. To preserve the linearity of problem formulation, the cost curve is thus approximated by using a piecewise linear function:

$$S_i^{PV\_SIZE} = m_i \cdot PV_i^{SIZE} + q_i \tag{5}$$

For each i segment, m slope and q intercept are defined (6):

$$\begin{cases} m_i = \left(S_{i+1}^{PV\_SIZE} - S_i^{PV\_SIZE}\right) / \left(PV_{i+1}^{SIZE} - PV_i^{SIZE}\right) \\ q_i \leq S_i^{SIZE} - m_i \cdot PV_i^{SIZE} \end{cases} \tag{6}$$

Interval constraints are defined to guarantee that S_{PV_SIZE} remains within the bounds of the active segment. Specifically, S_{PV_SIZE} must be greater/equal to the lower bound of the active segment and smaller/equal to the upper bound, as in (7)

$$\begin{cases} S_i^{PV\_SIZE} \geq PV_i^{SIZE} \cdot b_i \\ S_i^{PV\_SIZE} \leq PV_{i+1}^{SIZE} \cdot b_i + (1 - b_i) \cdot M \end{cases} \tag{7}$$

where b represents a binary variable. To ensure that only one segment is active at a time, constraint in (8) is imposed:

$$\begin{cases} S_i^{PV\_SIZE} \leq m_i \cdot PV_i^{SIZE} + q_i + (1 - b_i) \cdot M \\ S_i^{PV\_SIZE} \geq m_i \cdot PV_i^{SIZE} + q_i - (1 - b_i) \cdot M \end{cases} \tag{8}$$

Here, M is a sufficiently large constant (Big-M method) to ensure that PV size lies in exactly one segment. In (8), the

following constraint is also added:

$$\sum_{i=0}^{N} b_i = 1 \tag{9}$$

The described linearization introduces an approximation error; however, as demonstrated in the sensitivity analysis, this error remains within acceptable limits and does not significantly affect the results.

By adopting the objective function (OF) in the second step of the algorithm, the PV size corresponding to the maximum NPV is found as a function of marginal savings:

$$\max NPV = \sum_{t=0}^{T\_PV} \frac{C_{(0)} - C_{PV\_SIZE}(1 - 0.01t) - C_{O\&M}}{(1+r)^t} - C_{0\_PV} \tag{10}$$

The optimization is repeated in an iterative way by increasing the PV size with step of 1 kWp. At the end, the algorithm returns the size that leads to the maximum NPV.

D. OPTIMAL BES SIZE

Once the optimal PV size is identified, an analogous procedure is applied to find the optimal BES size. In this case, the BES power scheduling is simulated for each BES size and for one year to get the cost curve, while assuming the deterministic knowledge of prices, load and PV production, considering the charging/discharging power of BES as decision variables and minimizing the following OF:

$$\min C = \sum_{t=0}^{T} (P_{grid\_in,\,t} \cdot \pi_{in,\,t} - P_{grid\_ex,\,t} \cdot \pi_{ex,\,t}) \cdot \Delta t \tag{11}$$

An example of the BES scheduling for 2023 year is shown in Fig. 6. Here, P_{BES} is positive during discharging and P_{grid} is positive if absorbed. By starting from the constraints (2) and (3) related to the exchange with the external grid, additional constraints for the BES are introduced. As in [20], the net power exchange with the BES is in (12), whereas binary variables are included in (13) and (14) to avoid simultaneous charging and discharging in the same period:

$$P_{BES} = P_{BES\_ch}\eta_{BES} - P_{BES\_di}/\eta_{BES} \tag{12}$$

$$\begin{cases} P_{BES\_di} \le u \cdot P_{BES\_di\_MAX} \\ P_{BES\_ch} \le (1-u) \cdot P_{BES\_ch\_MAX} \end{cases} \tag{13}$$

$$SOC_t = SOC_{t-1} + (P_{BES}/E_{BES,\max}) \cdot \Delta t \tag{14}$$

SOC constraint in (14) and its limits, with initial/final values are included as in the following:

$$0.1 \le SOC_t \le 1, \tag{15}$$

$$[SOC_0 = SOC_{end} = 0.5]$$

In the BES scheduling, no constraints are imposed on the degradation of the batteries over time. This can lead to a moderate overestimation of BES usage and revenue. This aspect will be taken into account in the second phase for NPV optimization by introducing a linear degradation in the OF (16) [33]. Before calculating the NPV, the cost curve is modeled as a function of BES size, incorporating savings due to the introduction of the PV (optimal size) and the annual marginal savings achieved by progressively increasing the BES capacity (with step of 5 kWh). This one is defined as S^{BES_SIZE}=C_{PV} - C_{BES_SIZE}, for each BES size in kWh. Then, the optimization in (16) is performed:

$$\max NPV = \sum_{t=0}^{T\_BES} \frac{(C_{PV} - C_{BES\_SIZE})(1 - Dt) - C_{O\&M}}{(1+r)^t} - C_{0\_BES} \tag{16}$$

This leads to optimized costs as a function of various BES sizes, iterating OF (16) for each BSE size. The coefficient D is to take into account, from an economic point of view, the degradation of the BES. Finally, the cost curve is linearized too, and the algorithm computes the size that maximizes the NPV.

As the cost curve (Fig. 7) is not linear and (as in the case of the PV size optimization), the optimization system is nonlinear too and non-convex. Therefore, the same linearization for the cost curve is performed with the piecewise linear function procedure indicated in the PV size optimization, as in Section III-C.

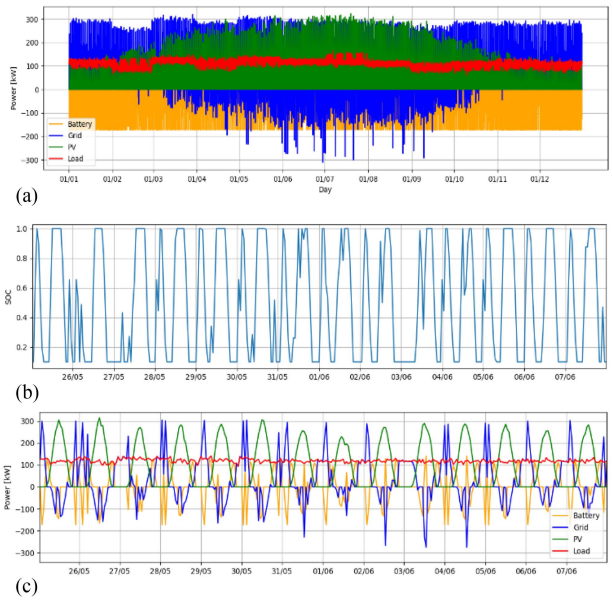

FIGURE 6. Power scheduling for 2023: (a) annual behavior of the BES power, grid exchange power, PV power production and power load; (b) SOC behavior of BES in two weeks; (c) behavior of the BES power, grid exchange power, PV power production and power load in two weeks [22].

IV. IMPLEMENTATION AND TEST RESULTS

The models have been implemented in Python and tested by using the library CVXPY [34], [35], and SCIPY [36] as a

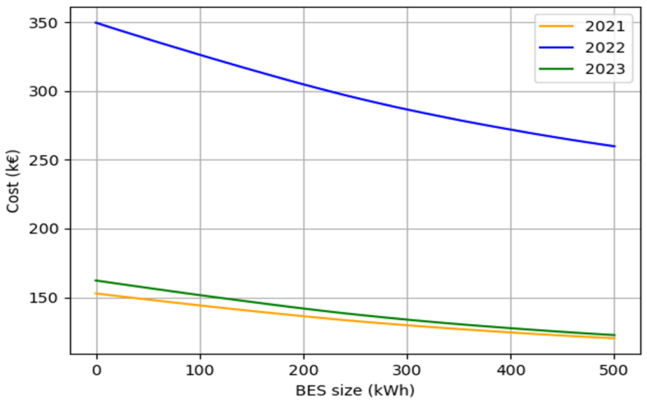

FIGURE 7. Energy cost as a function of the BES size (from 0 to 500 kWp) considering NSP of 2021, 2022 and 2023 [22].

TABLE 2. NPV Optimization, PV Optimal Size and Costs

Year	Optimal Size (kWp)	Optimal NPV (k€)	$C_{(0)}$ (k€/Year)	C_{PV} (k€/Year)	Savings %
2021	326	939.453	235.234	136.710	41.88
2022	500	5289.257	589.545	218.436	62.95
2023	341	991.044	245.716	142.072	42.18

solver of the MILP program on a 4.7-GHz Intel-i7 computer with 16 GB of RAM, running 64-bit Windows 11. All the calculations refer to a time window of one year, split into 8760 periods of 1 hour each. The results are offered in next tables.

For each of the considered years, results of PV optimal size along with the corresponding NPV, initial bill costs (without PV, assumed as a reference) and costs including PV (using optimal size) are provided in Table 2. The computation is performed in the PV size interval between 0 and 500 kWp, assuming CAPEX of 2 k€/kWp (including project, installation and grid connection), OPEX of 70 €/kWp per year, PV lifetime $T_{PV} = 25$ years and converter efficiency $\eta_{AC/DC} = 0.92$. The obtained results are able to show an optimal size of 326 and 341 kWp in the years 2021 and 2023 respectively, while the size tends to the full scale in 2022. The NPV in 2022 is also much higher (over 5 times that of the other years). This is essentially due to the very high NSP in 2022. High NSP price levels increase revenues from energy sales, largely offsetting procurement costs and resulting in higher NPVs; in turn, higher NPVs support the deployment of larger PV capacities. This represents an exceptional price and therefore it will not be considered. The PV size is then chosen as an average between 2021 and 2023, thus 334 kWp (i.e., size used in next steps). The PV size is compatible with the available surface area on the roof of the factory. The Table 3 provides the results of the second step optimization. Over the same three years, important data are represented, thus the NPV corresponding to the optimal BES size, the starting bill costs (with PV and without BES, assumed as a reference) and the costs including BES. The computation is performed in the BES capacity

TABLE 3. NPV Optimization, BES Optimal Size and Costs

Year	Optimal Size (kWh)	Optimal NPV (k€)	C_{PV} (k€/Year)	C_{BES} (k€/Year)	Savings %
2021	230	25.326	152.939	134.159	12.28
2022	500	473.386	349.630	259.827	25.69
2023	310	67.225	162.289	133.137	17.96

size interval between 0 and 500 kWh, assuming CAPEX of 0.5 k€/kWh (including project and installation), OPEX of 1 k€/year, the BES lifetime equal to T_{BES}=10 years, efficiency $\eta_{AC/DC} = 0.92$ and BES efficiency $\eta_{BES} = 0.90$. Similar considerations to those of previous case can be repeated for the choice of optimal BES size. Also in this case, the result for 2022 will not be considered, as it tends to the full scale (500 kWh) due to the very high NSP. The proposed optimal size for the BES is 270 kWh, that is the average resulting in the two years (2021 and 2023) with regular prices.

The numerical simulation presented concerns the Italian market, but the algorithm used is believed to be robust and applicable to any type of market. Economic signals, which serve as inputs to the optimization algorithm, implicitly govern the charging and discharging behavior of the BES through price differentials. In particular, PV generation is assumed to have a zero marginal cost, while energy injected into the grid is remunerated at the wholesale market price (NSP). Conversely, energy withdrawn from the grid is priced at twice the NSP to account for system charges, network fees, and taxes. Under these assumptions, charging the BES using grid electricity is economically unattractive. As a result, the optimization naturally prioritizes charging from on-site PV generation and subsequently discharging to the grid. In scenarios with fixed tariffs, capacity-based pricing, or negative market prices, the algorithm still minimizes procurement costs, only the strategy governing energy exchanges with the grid changes. However, there may be situations and markets in which the NPV is negative, and the BES investment is not convenient.

A. SENSITIVITY ANALYSIS

To assess how the NPV and the optimal size of the BES respond to variations in key input parameters, a sensitivity analysis was conducted. In particular, the analysis examined the effects of the discount rate r (ranging from 1% to 5%), the BES degradation rate D (ranging from 1% to 5%), considering in OF (16) a drop in revenue due to the loss of capacity, and the load standard deviation SD (ranging from 1 to 5 from the daily mean). The results are shown in Figs. 8 and 9.

The results indicate that increases in both the discount rate and the degradation rate led to an almost linear reduction in the NPV and the optimal BES size. The point at which the NPV becomes zero, beyond which the investment is no longer worthwhile, has also been calculated: NPV becomes zero for $r = 11\%$ and $D = 9.5\%$. The variations in the load standard deviation SD have only a marginal impact on the

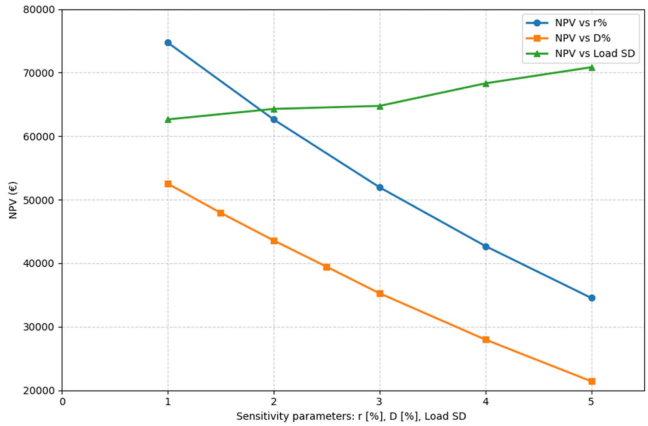

FIGURE 8. NPV sensitivity analysis as a function of discount rate (*r*), degradation rate (*D*) and load standard deviation (*SD*).

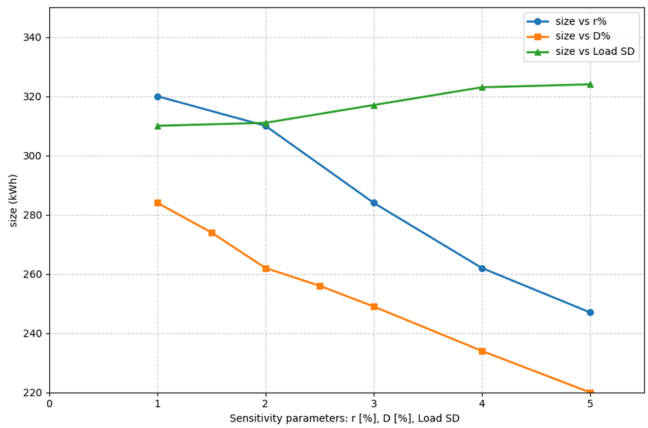

FIGURE 9. Optimal size of the BES sensitivity analysis as a function of discount rate (*r*), degradation rate (*D*) and load standard deviation (*SD*).

optimal size, which remains nearly constant. This outcome is expected, as the sizing decision is weakly dependent on power load variability: the primary role of the BES is to shift energy from periods of high PV generation to periods of low or absent generation (e.g., Fig. 6), largely independent of short-term load fluctuations. Additional simulations were carried out to assess the impact of the error introduced by the linearization of the cost curve of the PV and BES. To this end, progressively finer piecewise linear approximations were adopted, and the resulting optimal sizes were compared. Over the capacity range from 0 to 500 kWp (kWh), the cost function was linearized using segment widths of 10, 1, 0.1, and 0.05 kWp (kWh), with the finest discretization taken as a reference for the "exact" cost function. The corresponding results are reported in Table 4 and show that the approximation error remains limited, confirming the accuracy of the adopted linearization approach. With a discount rate of 3% the error committed is only 0.13% and 0.14% in the case of the PV size and the BES size respectively.

TABLE 4. Capacity PV and BES Optimization. Deviations Due to Linearization Cost Curve

PV Capacity step (kWp)	PV Size r = 3%	Deviation (%)	PV Size r = 4%	Deviation (%)
10	340	-0.42%	300	-0.06%
1	**341**	**-0.13%**	**300**	**-0.06%**
0.1	341.4	-0.01%	300.6	0.14%
0.05	341.45	0.00%	300.17	0.00%
BES Capacity step (kWh)	**BES Size r = 3%**	**Deviation (%)**	**BES Size r = 4%**	**Deviation (%)**
10	280.00	-0.92%	260.00	-1.25%
1	**283.00**	**0.14%**	**263.00**	**-0.11%**
0.1	282.60	0.00%	263.80	0.19%
0.05	282.60	0.00%	263.30	0.00%

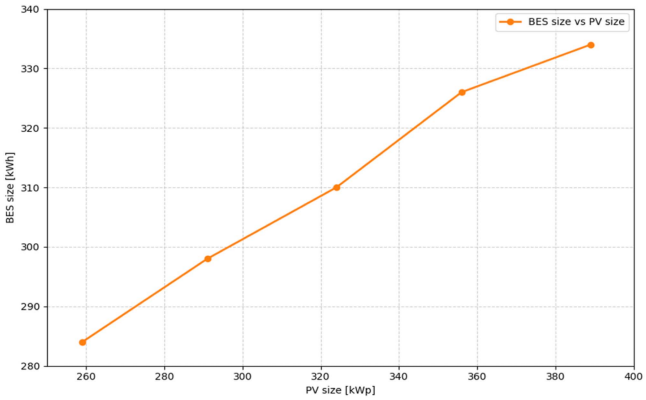

FIGURE 10. BES size behavior as a function of PV size.

With regard to the relationship between PV and BES sizing, the simulations reveal an approximately linear correlation between the two. When the PV capacity is varied within a ±20% range around its optimal value, the resulting trend shown in the following Fig. 10 is obtained.

To assess the robustness of the load profile used in the model, additional annual load profiles were generated based on the characteristics of the electroplating process. In particular, the plating process duration, ON-time period, was assumed to vary between 1 and 20 hours, depending on the required coating thickness, while the OFF-time ranged between 1 and 6 hours, reflecting loading and unloading operations. Multiple synthetic load profiles were constructed by aggregating the demand of the five electroplating tanks of the factory, each with different power ratings and operating independently according to randomly generated ON/OFF cycles within the specified ranges. The resulting dataset was normalized to preserve the same total annual energy consumption. The results, reported in Table 5, are consistent with those obtained using Gaussian noise-based perturbations, confirming the robustness of the proposed modeling approach.

The PV and BES sizing results obtained with different load profiles are consistent, with maximum deviations of 4.11% and 4.84%, respectively. This indicates that the optimal sizing is only weakly influenced by variations in the instantaneous

TABLE 5. Capacity PV and BES Optimization (year 2023) with Different Profiles Based on Monthly Bill and on Work Cycles

Profile	Work Cycle (h)	Rated Power for Each Tank (% P_{load})	PV Size (kWp)	BES Size (kWh)
Gaussian Noice	No Work Cycle	Tolal Power	341	310
Shift-Based 1	1-20 (ON) / 2-5 (OFF)	7, 14, 21,26, 32	350	317
Shift-Based 2	1-15 (ON) / 1-6 (OFF)	10, 30, 30, 20, 10	355	325

load profile and is primarily determined by the total energy demand (i.e., the integral of the power over time).

V. DC VOLTAGE CONTROL SYSTEM

The previous analysis primarily focused on the system from an energy balance perspective, while the control aspects were not addressed. This section examines the control and coordination strategies of the various power electronic interfaces. The objective is to ensure stable and flexible operation of the analyzed power system, as illustrated in Fig. 2. The control of the DC bus voltage is assigned to the BES converter, since the battery is capable of both absorbing and supplying power, thereby maintaining a constant power balance on the DC bus. Conversely, both the PV and grid-side converters operate under power control. This configuration enables the regulation of power exchange between the microgrid and the main grid, providing support during periods of insufficient PV generation and allowing energy export to the grid in case of excess production. To ensure that the proposed control strategy can guarantee stable operation and properly manage the power balance in the power system, it has been tested in a real-time capable circuit simulator.

To evaluate the proposed control strategies, a simulation setup was developed on the Typhoon HIL 604 platform. In this environment, the power electronic interfaces of the system and their associated control schemes were modeled in detail. The power electronics components are emulated with a simulation time step of 50 μs, while the execution rate of the control tasks is equal to 100 μs. This setup enables the assessment of the system's transient response under various perturbations.

Specifically, two test scenarios were conducted. The first test analyzes the transition from full PV supply to complete power supply from the grid. The second test examines the transition from islanded operation to grid-connected mode, where the excess generated power is exported to the grid. The test scenarios analyzed in this work represent ordinary operating conditions, as the focus of this paper is on the proposed energy management strategy. Fault conditions or sudden load losses are therefore outside the scope of this study and have not been investigated. Nevertheless, considering the critical role of protection coordination in DC power systems, this aspect will be addressed in future works. The first test is illustrated in Fig. 11. The electroplating facility requires a power demand of 200 kW (purple line in the power transient

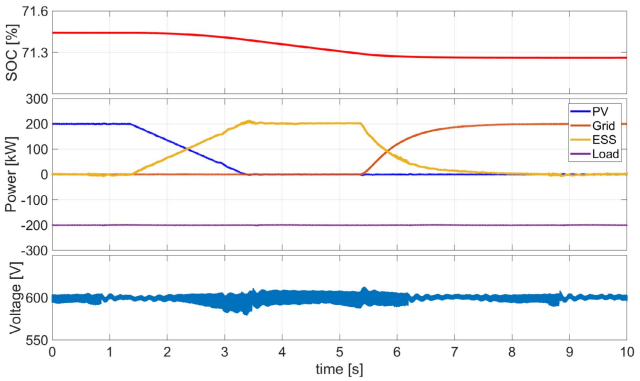

FIGURE 11. Switch from PV supply to grid supply: SOC, power and voltage transients.

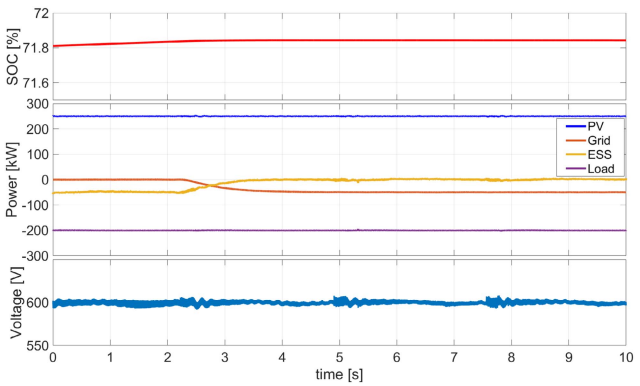

FIGURE 12. Switch from islanded mode to energy injected to the grid: SOC, power and voltage transients.

of Fig. 11). Initially, this load is entirely supplied by the PV system (blue line). At 1.5 s, the PV system is gradually disconnected as solar irradiance decreases, and at 5.5 s, the grid begins to fully supply the load. During this transient period, the storage system temporarily supports the load, as indicated by the SOC shown in the top section of Fig. 11. The DC bus voltage is also depicted; as shown in the third section of Fig. 11, the battery effectively maintains a stable bus voltage throughout the transition.

The second test concerns the transition from islanded to grid-connected operation, and the corresponding transients are shown in Fig. 12. The system operates in steady state with a PV output of 250 kW (blue line in the power transient of Fig. 12), which is sufficient to supply the 200 kW load and simultaneously charge the battery. However, since the battery SOC is already above 70% (red line in Fig. 12), the excess power can be exported to the grid. Specifically, at approximately 2 s, 50 kW of surplus power are redirected to the external grid (orange transient), while the storage system continues to regulate the DC bus voltage, maintaining an almost constant SOC. As in the previous test, the bus voltage regulation is ensured by the storage system, as shown in the third section of Fig. 12.

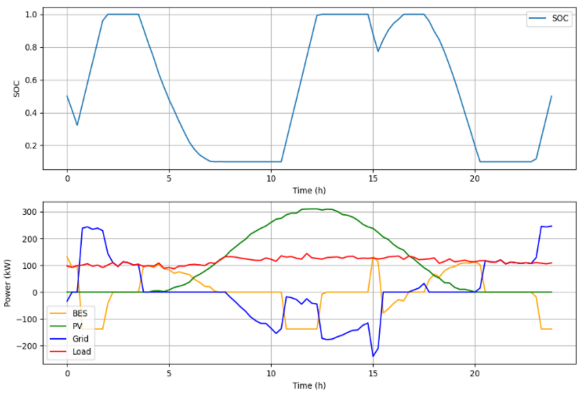

FIGURE 13. EMS power scheduling for a summer day: behavior of the BES SOC (upper part) and BES power, grid exchange power, PV power production and load power (lower part) [8].

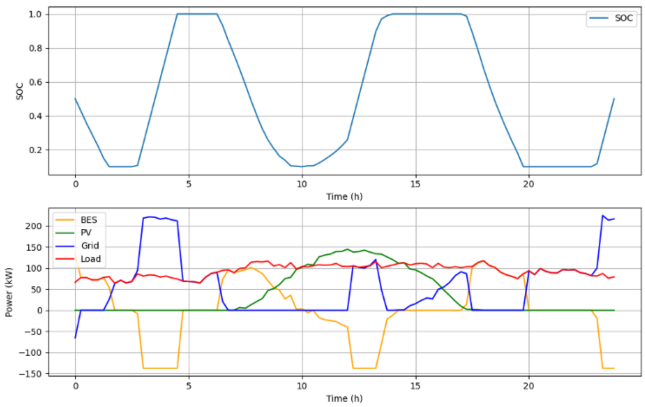

FIGURE 14. EMS power scheduling for a winter day: behavior of the BES SOC (upper part) and BES power, grid exchange power, PV power production and load power (lower part).

VI. ENERGY MANAGEMENT SYSTEM

From [8], next subsection explains the EMS for the case under study. The optimization procedure relies on input data consisting of load profiles and PV production forecasts, both evaluated one day in advance. Moreover, also the NSP published the previous day by the electricity market operator is utilized. Based on this information, the algorithm schedules BES optimal power for the next day. The proposed MILP-based optimization adopts the same objective function (OF) and set of constraints previously defined for the annual scheduling model. In particular, OF (10) minimizes the cost of energy exchanged with the main grid, while assuming that injected energy is sold at the NSP and withdrawn energy is purchased at a price equal to twice the NSP. The scheduling horizon spans 24 hours, divided into 96 intervals (Δt) of 15 minutes each. The system operates subject to the grid constraints defined by (1)–(3) and the BES constraints defined by (12)–(15). Within this framework, the optimization algorithm performs day-ahead scheduling of BES power by allocating dispatch across the 96 time intervals. Figs. 13 and 14 illustrate the scheduled state of charge (SOC) and power profiles for two representative days, one in summer and one in winter.

The results are obtained using the optimal BES size determined by the proposed algorithm. As an example, the load demand, PV generation, and NSP forecast profiles are shown for a typical summer day (4 July 2023) and a typical winter day (9 February 2023) [8]. As in Figs. 13 and 14, the BES charges not only during periods of PV generation surplus but also during nighttime hours when electricity prices are lower, thus showing a key advantage of EMS optimization method.

The proposed EMS adopts a hierarchical control architecture. Day-ahead scheduling is first performed over a 24-hour horizon using forecasted PV generation and load profiles. To manage real-time deviations from these forecasts, a receding-horizon control strategy, conceptually aligned with Model Predictive Control (MPC), is implemented using the same optimization model. The optimization problem is periodically re-solved throughout the day based on updated measurements and short-term forecasts, while only the first control action is applied at each iteration [37] [38]. The real-time corrective layer acts on fast operational variables, such as BES charging and discharging power and grid exchange, ensuring constraint satisfaction and mitigating forecast-induced deviations while preserving the economic optimality of the day-ahead plan. Long-term decisions, including system sizing and contractual arrangements, remain unchanged. Short-term uncertainty, including forecast errors in PV generation and load demand, is managed through the receding-horizon EMS, which updates control actions in real time to ensure feasibility and operational robustness. The EMS is executed multiple times during the day to account for variations in PV generation and deviations in the expected state of charge, generating corrective setpoints for the power management system (PMS) of the electroplating facility.

Given the adopted control strategy, corrective actions are limited to defining the power setpoint of the grid-side converter, while the BES converter maintains DC bus voltage regulation and compensates for deviations from the rated bus voltage. This tertiary control layer can be integrated into Typhoon HIL simulations through an external controller, enabling a controller hardware-in-the-loop (CHIL) configuration [7], [39], [40], [41]. In this setup, the EMS receives real-time measurements of power setpoints, state-of-charge values, and PV power output, processes these inputs through the EMS algorithm, and transmits updated control commands to the PMS, allowing realistic validation of control strategy under dynamic operating conditions.

VII. CONCLUSION

This paper investigates the introduction of a DC microgrid in industrial environments that already make extensive use of direct current, such as electroplating plants.

In this context the cost savings related to optimized energy procurement of a DC Microgrid for Electroplating Industry are discussed. The proposed configuration, based on a common DC bus interconnecting PV, BES and DC loads, allows

to interface the DC MG with a commercial solar hybrid inverter, then avoiding the expense of additional converters to the external AC grid. The case study is noteworthy taking into account the large amount of energy that characterizes the electroplating galvanic processes of considered factory. A two steps linear optimization procedure is proposed that provides optimal of PV and BES sizing to maximize the net present value of investments savings. Also, the differences and consequences due to the great swing in national single price of three reference years are discussed in detail.

The proposed DC microgrid layout is characterized by a lower initial investment cost, which influences the optimal sizing of PV and BES systems. Moreover, the DC MG solution can ensure better power quality and efficiency are expected with respect to standard AC.

Also, the energy management system is explored. The same MILP structure is consistently used across planning (annual horizon) and operational (day-ahead and real-time horizon) levels, enabling methodological coherence between sizing and EMS implementation. The integration of the sizing procedure with a hierarchical EMS architecture including receding-horizon control further strengthens the practical applicability of the framework.

In the paper, particular attention is spent to highlight the DC voltage control in the transition among different operative conditions. A complete test on HIL platform is detailed to verify the microgrid operation, while providing voltage/power/SOC of the designed DC microgrid system.

ACKNOWLEDGMENT

The authors wish to thank Typhoon HIL for providing the platform used in the development of this research work.

REFERENCES

[1] European Union, "Directive UE 2018/2001 on the promotion of the use of energy from renewable sources," 2018. [Online]. Available: https://eur-lex.europa.eu/legal-content/EN/TXT/PDF/?uri=CELEX:32018L2001from=EN

[2] European Parliament, "Establishing a framework of measures for strengthening Europe's net-zero technology manufacturing ecosystem and amending regulation," Regulation (EU) 2024/1735. [Online]. Available: https://eurlex.europa.eu/eli/reg/2024/1735/2025-08-17/eng

[3] Directive (EU) 2023/1791 of the European Parliament and of the Council of 13 September 2023 on energy efficiency and amending Regulation (EU) 2023/955 (recast). [Online]. Available: https://eur-lex.europa.eu/eli/dir/2023/1791/oj/eng

[4] S. Ferahtia, A. Houari, T. Cioara, M. Bouznit, H. Rezk, and A. Djerioui, "Recent advances on energy management and control of direct current microgrid for smart cities and industry: A survey," *Appl. Energy*, vol. 368, Aug. 2024, Art. no. 123501.

[5] K. Jithin, P. P. Haridev, N. Mayadevi, R. P. Harikumar, and V. P. Mini, "A review on challenges in DC microgrid planning and implementation," *J. Modern Power Syst. Clean Energy*, vol. 11, no. 5, pp. 1375–1395, Sep. 2023.

[6] D. Bosich, M. Chiandone, G. Sulligoi, A. A. Tavagnutti, and A. Vicenzutti, "High-performance megawatt-scale MVDC zonal electrical distribution system based on power electronics open system interfaces," *IEEE Trans. Transport. Electrific.*, vol. 9, no. 3, pp. 4541–4551, Sep. 2023.

[7] A. A. Tavagnutti, D. Bosich, M. Chiandone, A. Vicenzutti, and G. Sulligoi, "Preventive-resilient algorithm based on weighted bandwidth method for stable load management in zonal DC microgrids," *IEEE Access*, vol. 12, pp. 166031–166043, 2024.

[8] S. Lilla et al., "DC microgrids for industrial DC application: focus on energy management and storage optimization," in *Proc. 2025 AEIT HVDC Int. Conf.* , 2025, pp. 1–6.

[9] M. Schlesinger and M. Paunovic, *Modern Electroplating*. Hoboken, NJ, USA: Wiley, 2011.

[10] N. Mahalanobis and D. Malecek, "Industrial implementation of environmentally friendly nanometal electroplating process for chromium and copper Beryllium replacement using low cost pulse current power supplies," *ESTCP Environ. Secur. Technol. Certification Prog.*, 2014. [Online]. Available: https://apps.dtic.mil/sti/tr/pdf/ADA619713.pdf

[11] N. V. Mandich and D. L. Snyder, "Electrodeposition of Chromium," in *Modern Electroplating*, M. Schlesinger and M. Paunovic, Eds., Wiley, 2010. [Online]. Available: https://doi.org/10.1002/9780470602638.ch7

[12] A. Leiden et al., "Model-based analysis, control and dosing of electroplating electrolytes," in *Proc. Int. J. Adv. Manuf. Technol.*, vol. 111, pp. 1751–1766, 2020. [Online]. Available: https://doi.org/10.1007/s00170-020-06190-0

[13] U. Manandhar, A. Ukil, and T. K. Jonathan, "Efficiency comparison of DC and AC microgrid," in *Proc. 2015 IEEE Innov. Smart Grid Technol. - Asia*, 2015, pp. 1–6.

[14] J. Kong, S. T. Kim, B. O. Kang, and J. Jung, "Determining the size of energy storage system to maximize the economic profit for photovoltaic and wind turbine generators in South Korea," *Renewable Sustain. Energy Rev.*, vol. 116, Dec. 2019, Art. no. 109467.

[15] A. Nottrott, J. Kleissl, and B. Washom, "Energy dispatch schedule optimization and cost benefit analysis for grid-connected, photovoltaic-battery storage systems," *Renewable Energy*, vol. 55, pp. 230–240, Jul. 2013.

[16] J. J. Kelly and P. G. Leahy, "Sizing battery energy storage systems: Using multi-objective optimization to overcome the investment scale problem of annual worth," *IEEE Trans. Sustain. Energy*, vol. 1, no. 4, pp. 2305–2314, Oct. 2020.

[17] G. S. Thirunavukkarasu, M. Seyedmahmoudian, E. Jamei, B. Horan, S. Mekhilef, and A. Stojcevski, "Role of optimization techniques in microgrid energy management systems—A review," *Energy Strategy Rev.*, vol. 43, Sep. 2022, Art. no. 100899.

[18] S. Ali, Z. Zheng, M. Aillerie, J. P. Sawicki, M. C. Péra, and D. Hissel, "A review of DC microgrid energy management systems dedicated to residential applications," *Energies*, vol. 14, no. 14, Jul. 2021, Art. no. 4308.

[19] S. Ahmad, M. Shafiullah, C. B. Ahmed, and M. Alowaifeer, "A review of microgrid energy management and control strategies," *IEEE Access*, vol. 11, pp. 21729–21757, 2023.

[20] S. Lilla, C. Orozco, A. Borghetti, F. Napolitano, and F. Tossani, "Day-ahead scheduling of a local energy community: An alternating direction method of multipliers approach," *IEEE Trans. Power Syst.*, vol. 35, no. 2, pp. 1132–1142, Mar. 2020.

[21] K. M. Bhargavi, N. S. Jayalakshmi, D. N. Gaonkar, A. Shrivastava, and V. K. Jadoun, "A comprehensive review on control techniques for power management of isolated DC microgrid system operation," *IEEE Access*, vol. 9, pp. 32196–32228, 2021.

[22] S. Lilla et al., "Technical-economic assessment of a DC microgrid for electroplating industry," in *Proc. IEEE 7th Int. Conf. DC Microgrids*, 2025, pp. 1–5.

[23] J. Meng et al., "Output voltage response improvement and ripple reduction control for input-parallel output-parallel high-power DC supply," *IEEE Trans. Power Electron.*, vol. 38, no. 9, pp. 11102–11112, Sep. 2023.

[24] P. Grzejszczak, K. Wolski, M. Szmczak, A. Czaplicki, and A. Sitnik, "Design of a 20-kW SiC-based phase-shifted DC/DC full bridge converter," in *Proc. 2021 Prog. Appl. Elect. Eng.*, 2021, pp. 1–5.

[25] W. Hang, L. Cheng, Z. Xingzhi, and Z. Yaoze, "Research on electroplating power supply based on three-phase interleaved parallel LLC resonant converter," in *Proc. 2023 IEEE Int. Conf. Control, Electron. Comput. Technol.*, Jilin, China, 2023, pp. 90–94.

[26] D. Bosich, M. Gibescu, and G. Sulligoi, "Large-signal stability analysis of two power converters solutions for DC shipboard microgrid," in *Proc. IEEE 2nd Int. Conf. DC Microgrids*, Nuremburg, Germany, 2017, pp. 125–132.

[27] Y. Pei, G. Jiang, H. Liu, and Z. Wang, "Development of high current power supply for electroplating," in *Proc. IEEE 33rd Annu. IEEE Power Electron. Specialists Conf.*, Cairns, QLD, Australia, 2002, pp. 21–23.

[28] A. N. Arvindan, M. A. Arshad Mohamed, and R. Aravind, "Power quality analysis of six- and twelve-pulse rectifiers as series cascaded topologies of the three-pulse rectifier," in *Proc. 2nd Int. Conf. Power Embedded Drive Control*, Chennai, India, 2019, pp. 383–389.
[29] E. Sakasegawa, R. Chishiki, R. Sedutsu, T. Soeda, H. Haga, and R. M. Kennel, "Comparison of interleaved boost converter and two-phase boost converter characteristics for three-level inverters," *World Electron. Veh. J.*, vol. 14, 2023, Art. no. 7.
[30] M. H. Rashid, *Power Electronics: Circuits, Devices, and Applications*, 4th ed. Noida, India: Pearson, 2014.
[31] M. Venkatesh Naik and P. Samuel, "Analysis of ripple current, power losses and high efficiency of DC–DC converters for fuel cell power generating systems," *Renewable Sustain. Energy Rev.*, vol. 59, pp. 1080–1088, 2016.
[32] GME, "Gestore mercati energetici (GME)," 2026. [Online]. Available: https://www.mercatoelettrico.org/en/
[33] A. Perez, R. Moreno, R. Moreira, M. Orchard, and G. Strbac, "Effect of battery degradation on multi-service portfolios of energy storage," *IEEE Trans. Sustain. Energy*, vol. 7, no. 4, pp. 1718–1729, Oct. 2016.
[34] S. Diamond and S. Boyd, "CVXPY: A python-embedded modeling language for convex optimization," *J. Mach. Learn. Res.*, vol. 17, no. 83, pp. 1–5, 2016.
[35] A. Agrawal, R. Verschueren, S. Diamond, and S. Boyd, "A rewriting system for convex optimization problems," *J. Control Decis.*, vol. 5, no. 1, pp. 42–60, 2018.
[36] P. Virtanen et al., "SciPy 1.0: Fundamental algorithms for scientific-computing in python," *Nature Methods*, vol. 17, pp. 261–272, 2020.
[37] J. Hu et al., "Economic model predictive control for microgrid optimization: A review," *IEEE Trans. Smart Grid*, vol. 15, no. 1, pp. 472–484, Jan. 2024.
[38] A. Parisio, E. Rikos, and L. Glielmo, "A model predictive control approach to microgrid operation optimization," *IEEE Trans. Control Syst. Technol.*, vol. 22, no. 99, pp. 1813–1827, Sep. 2014.
[39] A. A. Tavagnutti, M. Chiandone, D. Bosich, and G. Sulligoi, "A stability-aimed PMS for shipboard zonal DC microgrids: The C-HIL tests on real-time platform," in *Proc. 2023 IEEE Electric Ship Technol. Symp.*, 2023, pp. 453–457.
[40] A. A. Tavagnutti, M. D. Feste, M. Chiandone, A. Vicenzutti, D. Bosich, and G. Sulligoi, "A decision support system for the stable real-time power management of onboard zonal DC microgrids," in *Proc. 2024 Open Source Modelling Simul. Energy Syst.*, 2024, pp. 1–6.
[41] A. A. Tavagnutti, A. Vicenzutti, M. Chiandone, D. Bosich, and G. Sulligoi, "The digital twin of complex shipboard DC microgrids: The high-performing synergy of compiled models and HIL platform in the dynamics emulation of zonal power electronic power distribution systems," *IET Power Electron.*, vol. 18, Jan. 2025, Art. no. e12835.

STEFANO LILLA (Member, IEEE) received the M.Sc. degree in electrical engineering and the Ph.D. degree in biomedical, electrical and systems engineering from the University of Bologna, Bologna, Italy, in 1996 and 2019, respectively. He is currently an Assistant professor with the University of Bologna. He is also a Consultant and Project Engineer in the renewable source and storage area. His research interests include decentralized and distributed control strategies for microgrids, energy communities, vehicle-to-grid (V2G) integration, battery energy storage systems and optimization modelling, and the techno-economic assessment of renewable energy systems coupled with storage.

ANDREA ALESSIA TAVAGNUTTI (Member, IEEE) received the M.Sc. (Hons.) degree in electrical engineering from the University of Trieste, Trieste, Italy, in 2020. She is currently an Assistant professor with the University of Trieste. Her research activity is carried out with the Digital Energy Transformation and Electrification Facility, Department of Engineering and Architecture, University of Trieste. Her main research interests include the field of marine power systems, voltage control and power systems stability.

DANIELE BOSICH (Senior Member, IEEE) received the M.Sc. (Hons.) degree in electrical engineering with the University of Trieste, Trieste, Italy, in 2010, and the Ph.D. degree in energy engineering with the University of Padua, Padua, Italy, in 2014. He is currently an Associate Professor of microgrids for the sustainable energy with the University of Trieste. He is the author of more than 100 papers in the field of marine shipboard power systems, microgrid modeling, voltage control, and nonlinear systems analysis. Dr. Bosich is a Senior Member of PES, IAS, IES, and VTS societies.

FABIO NAPOLITANO (Senior Member, IEEE) received the M.S. and Ph.D. degrees in electrical engineering from the University of Bologna, Bologna, Italy, in 2009. He is currently an Associate Professor with the Department of Electrical, Electronic and Information Engineering, University of Bologna. His research interests include the analysis of power systems transients, in particular those due to indirect lightning strokes, and lightning protection systems. He is member of Technical Committee 81 of Italian Electrotechnical Committee. He is Associate Editor of IEEE TRANSACTIONS ON ELECTROMAGNETIC COMPATIBILITY.

ANDREA PREVEDI received the M.Sc. degree in electrical engineering and the Ph.D. degree in biomedical, electrical, and systems engineering from the University of Bologna, Bologna, Italy, in 2020 and 2025, respectively. He is currently an energy grid planning Specialist with the Smart Infrastructure Unit, Unareti S.p.A. His main research interests include renewable energy integration in modern power systems, with a focus on energy communities, battery storage systems, and inertia estimation in the presence of power converters.

FABIO TOSSANI (Senior Member, IEEE) received the B.S. (Hons.), M.S. (Hons.), and Ph.D. degrees in electrical engineering from the University of Bologna, Bologna, Italy. He is currently an Associate Professor with the Department of Electrical, Electronic, and Information Engineering "Guglielmo Marconi", University of Bologna. His research interests include the challenges and opportunities of modern power systems, with particular emphasis on power system transients, including the impact of lightning phenomena on electrical networks, and advancements in power system protection. Dr. Tossani is also dedicated to advancing sustainable energy solutions, with a focus on developing models to support efficient, self-sustaining energy communities. He is the Editor of *Electric Power Systems Research*.

GIORGIO SULLIGOI (Senior Member, IEEE) received the M.Sc. (Hons.) degree in electrical engineering from the University of Trieste, Trieste, Italy, in 2001, and the Ph.D. degree in electrical engineering from the University of Padua, Padua, Italy, in 2005. He is currently the Founder and Director of the Digital Energy Transformation & Electrification Facility, Department of Engineering and Architecture, University of Trieste. He is also a Full Professor of electric power generation and control and appointed Full Professor of shipboard electrical power systems. He is the author of more than 200 scientific papers in the fields of shipboard power systems, all-electric ships, generators modeling, and voltage control.

CARLO ALBERTO NUCCI (Life Fellow, IEEE) is currently a Full Professor with the University of Bologna, Bologna, Italy. He is currently a Doctor Honoris Causa with the University of Bucharest, Bucharest, Romania, Member of Italian scientific academies, and a Distinguished Invited Professor with Tsinghua University, Beijing, China, from 2023 to 2026. He is the author of more than 460 scientific articles and 13 book chapters on topics such as lightning protection of electrical systems, blackout@#@s, smart grids, smart cities and energy communities. He is also the Italian Representative in the HE Mission "Climate-Neutral and Smart cities", as the Chair of the International Conference on Lightning Protection, ICLP, as Co-Chair of the International Conference on Power Systems Transients, IPST and as Vice-Chair of the Ex-Board of the Power Systems Computation Conference, PSCC. He is a CIGRE Fellow and CSEE Fellow. He was the recipient of international awards, including the CIGRE Technical Committee Award.